






Quantum-optical excitations of semiconductor nanostructures in a microcavity using a two-band model and a single-mode quantum field

H. Rose ^{1,2}, A. N. Vasil'ev ³, O. V. Tikhonova ⁴, T. Meier ^{1,2} and P. R. Sharapova ¹

¹*Department of Physics, Paderborn University, Warburger Straße 100, D-33098 Paderborn, Germany*

²*Institute for Photonic Quantum Systems (PhoQS), Paderborn University, Warburger Straße 100, D-33098 Paderborn, Germany*

³*Institute of Nuclear Physics, Moscow State University, Leninskie Gory, 1, Moscow 119991, Russia*

⁴*Faculty of Physics, Moscow State University, Leninskie Gory, 1, Moscow 119991, Russia*



(Received 25 July 2022; accepted 12 December 2022; published 4 January 2023)

We theoretically study quantum-optical properties of one- and two-dimensional semiconductor nanostructures, where the electronic band structure is described by a two-band tight-binding model. Since the focus of our work is on analyzing quantum-optical effects of systems with a continuous band structure, many-body processes like electron-electron and electron-phonon interactions are neglected. The quantum-optical interband excitations are fully incorporated and described by a Jaynes-Cummings-type model. The exciting quantum light can be a state with arbitrary photon statistics. For simplicity, the results discussed here are limited to single-photon and two-photon Fock states. Our analytical approach is based on the eigenvalue problem and can be utilized to obtain explicit expressions for the steady-state properties of the system. Numerical simulations are based on solutions of the equations of motion and allow for a more precise analysis of the dynamics and nonresonant excitations of the system. We demonstrate that during the interaction process, a collective excitation of the conduction band is formed. For nonresonant excitations, this collective dynamics results in interesting steady states, in which the resonantly addressed eigenstates are occupied. The presented model provides a framework for microscopic simulations of quantum-optically excited extended semiconductor nanostructures.

DOI: [10.1103/PhysRevA.107.013703](https://doi.org/10.1103/PhysRevA.107.013703)

I. INTRODUCTION

Several effects that arise due to the interaction between quantum light and matter can be understood by treating the matter as atomic few-level systems [1]. The consideration of such systems is beneficial since they often allow one to obtain exact solutions due to the limited degrees of freedom and, at the same time, have led to significant progress in the fields of quantum computing, quantum information, and quantum cryptography [2–4]. On the other hand, quantum-optical excitations of extended semiconductors have given rise to a new branch in science, namely, semiconductor quantum optics [5], where concepts of both optics and many-body theory need to be systematically combined. Semiconductors excited by quantum light show different properties [6] and are very promising candidates for novel quantum devices [5], which, however, require more involved theoretical descriptions and usually demand approximation methods, such as the cluster-expansion approach [7]. Over the past few decades, attention has focused on semiconductor nanostructures, which are semiconductors of a reduced geometry in which the carriers are confined in a certain number of dimensions. This number determines the type of semiconductor nanostructure, leading to quantum dots, quantum wires, and quantum wells, which are quasi-zero-dimensional materials, quasi-one-dimensional (quasi-1D) materials, and quasi-two-dimensional (quasi-2D) materials, respectively [8,9]. These structures are accompanied by unique optical properties and have led to a number of promising applications [9–18].

Here, we study quantum-optical properties of 1D and 2D semiconductor nanostructures, i.e., quantum wires and quantum wells which are extended in one or two dimensions, respectively, whose electronic band structure are described by a tight-binding model [17,19,20]. Although we neglect the Coulomb interaction and the interaction with phonons [5,21,22], for the latter we assume very low temperatures at which the relaxation time is sufficiently long, as was shown for quantum well systems [23]; we explicitly take into account the photon statistics of the quantum light, which leads to a many-body problem itself. We present a theoretical approach that includes quantum light with arbitrary photon statistics. Clearly, the numerical complexity of the problem, i.e., the number of coupled equations of motion, greatly and rapidly increases with the number of photons. Therefore, we will mainly restrict our analysis to single-photon states, which can be efficiently generated and constitute an important building element for quantum information and quantum cryptography protocols [24–29], but also consider two-photon states. We start with an analytical treatment of the system, in which we obtain its general properties and derive explicit expressions for the ground-state probability. Afterwards, we show and discuss results of numerical simulations of the equations of motion to highlight the microscopic behavior of the system.

II. THEORETICAL MODEL

The microscopic description of semiconductor nanostructures is performed using a two-band model, in which for each

k point only vertical transitions are allowed. Thus, the total Hamiltonian describing the interaction of such a system with a single-mode quantum light is composed of the electronic band structure of the semiconductor, the quantum-light mode, and the interaction term in the dipole and rotating-wave approximation, which corresponds to a Jaynes-Cummings-type model:

$$\hat{H} = \sum_{\mathbf{k}} [\epsilon_{\mathbf{k}}^v a_{v,\mathbf{k}}^\dagger a_{v,\mathbf{k}} + \epsilon_{\mathbf{k}}^c a_{c,\mathbf{k}}^\dagger a_{c,\mathbf{k}}] + \hbar v \left[b^\dagger b + \frac{1}{2} \right] - \sum_{\mathbf{k}} M_{\mathbf{k}} (b^\dagger a_{v,\mathbf{k}}^\dagger a_{c,\mathbf{k}} + b a_{c,\mathbf{k}}^\dagger a_{v,\mathbf{k}}), \quad (1)$$

where $a_{\gamma,\mathbf{k}}^\dagger$ ($a_{\gamma,\mathbf{k}}$) is the creation (annihilation) operator of an electron with momentum \mathbf{k} in the band γ , while $\epsilon_{\mathbf{k}}^\gamma$ is the γ -band energy corresponding to momentum \mathbf{k} , where $\gamma = v$ denotes the valence band and $\gamma = c$ denotes the conduction band. b^\dagger (b) is the creation (annihilation) operator of a photon in the quantum-optical mode that excites the semiconductor, $M_{\mathbf{k}}$ is the light-matter coupling, and v is the frequency of the quantum-light mode, which in the scope of this work is assumed to be constant. To ensure that different band discretizations do not lead to different dynamics, the total oscillator strength of the system is kept constant by using $M_{\mathbf{k}} = M_0/\sqrt{N}$, where N is the number of k points. Thus, rather than $M_{\mathbf{k}}$, the relevant quantity for this system is M_0 . Note that the factor of $1/\sqrt{N}$ originates from preserving the commutation relations for the creation and annihilation operators for different discretizations of the k space [30].

To simplify the notation in the subsequent description and equations, we introduce the compound index γ , which contains the band indices for the N considered k points, i.e., $(\gamma) = \gamma_1, \gamma_2, \dots, \gamma_N$, where γ_j can be either v or c . To denote a change that is applied to this index, the following notation is introduced:

$$\gamma_1, \gamma_2, \dots, \gamma_{j-1}, \gamma_j \pm 1, \gamma_{j+1}, \dots, \gamma_N = (\gamma|\gamma_j \pm 1), \quad (2)$$

$$\gamma_1, \gamma_2, \dots, \gamma_{j-1}, \tilde{\gamma}, \gamma_{j+1}, \dots, \gamma_N = (\gamma|\gamma_j = \tilde{\gamma}), \quad (3)$$

where $+1$ and -1 describe the promotion and demotion of an electron in terms of the energy band, i.e., $v+1 = c$ and $c-1 = v$. At the same time, to denote that all k points are in their ground state we use $(v) = v, v, \dots, v$.

To obtain equations of motion that describe the considered system, we use the state-vector formalism. The state vector can be written as an expansion over basis vectors:

$$|\Psi\rangle = \sum_{(\gamma)} \sum_{n=0}^{\infty} c_n^{(\gamma)} e^{\frac{i}{\hbar} E_n^{(\gamma)} t} |(\gamma), n\rangle. \quad (4)$$

Here, $c_n^{(\gamma)}$ is the probability amplitude for the system to be in the state $|(\gamma), n\rangle$, where n is the Fock-state number of the quantum-light mode and $E_n^{(\gamma)}$ is the corresponding energy. The equations of motion for the probability amplitudes $c_n^{(\gamma)}$ can be derived from the Schrödinger equation and

read

$$-i\hbar\partial_t c_n^{(\gamma)} = \sum_{j=1}^N M_{k_j} c_{n-1}^{(\gamma|\gamma_j+1)} e^{-\frac{i}{\hbar}\Delta_{k_j} t} \sqrt{n}\delta_{\gamma_j,v} + \sum_{j=1}^N M_{k_j} c_{n+1}^{(\gamma|\gamma_j-1)} e^{\frac{i}{\hbar}\Delta_{k_j} t} \sqrt{n+1}\delta_{\gamma_j,c}, \quad (5)$$

where j constitutes the discretization index for the continuous k space. The optical detuning $\Delta_{\mathbf{k}}$ is given by

$$\Delta_{\mathbf{k}} = \hbar(\omega_{\mathbf{k}} - v), \quad (6)$$

$$\hbar\omega_{\mathbf{k}} = \epsilon_{\mathbf{k}}^c - \epsilon_{\mathbf{k}}^v, \quad (7)$$

where $\omega_{\mathbf{k}}$ determines the band structure and reflects the material properties, such as composition and dimensionality. In this work, we focus on 1D and 2D tight-binding models. Thus, in the 1D case, the band structure is given by

$$\omega_{\mathbf{k}} = \omega_g + \frac{\omega_b}{2} [1 - \cos(ka)], \quad (8)$$

where $\hbar\omega_g$ determines the energy gap, $\hbar\omega_b$ is the bandwidth, and a is the lattice constant. These three values are material parameters, and for example, for GaAs-based structures, typical values are given by $\hbar\omega_g = 1.5\text{eV}$, $\hbar\omega_b = 1.8\text{eV}$, and $a = 5.65\text{\AA}$. The band structure in the 2D case reads

$$\omega_{\mathbf{k}} = \omega_g + \frac{\omega_b}{4} [2 - \cos(k_x a) - \cos(k_y a)]. \quad (9)$$

This does not correspond to the zinc-blende crystal structure of GaAs which results in a fcc lattice in k space, but rather describes a cubic crystal structure. However, this simplification does not significantly modify the results shown below as they are dominated by the parabolic region of the band structure near the band gap.

In this work, we mainly focus on the occupation probabilities. For this, we determine the ground-state probability (GSP) O_{ground} as the probability that the semiconductor is in its electronic ground state; initially, this probability is equal to 1. Other relevant measures are the conduction- and valence-band occupation probabilities for a fixed k point k_j , namely, $O_c^{k_j}$ and $O_v^{k_j}$, respectively, which are obtained by tracing out all other k points and the light mode. These observables can be computed from the probability amplitudes and read

$$O_{\text{ground}} = \sum_{n=0}^{\infty} |c_n^{(v)}|^2, \quad (10)$$

$$O_c^{k_j} = \sum_{n=0}^{\infty} \sum_{\gamma \neq \gamma_j} |c_n^{(\gamma|\gamma_j=c)}|^2, \quad (11)$$

$$O_v^{k_j} = \sum_{n=0}^{\infty} \sum_{\gamma \neq \gamma_j} |c_n^{(\gamma|\gamma_j=v)}|^2, \quad (12)$$

where $O_c^{k_j} + O_v^{k_j} = 1$, which follows from the trace conservation of the corresponding density matrix.

In general, arbitrary photon statistics can be applied for the quantum-light mode. However, the more photons that are involved, the more extensive the many-body problem becomes, which can rapidly exceed tasks that can be solved by classical computers, as was similarly concluded for spin systems

[31,32] and quantum dots in microcavities considering Dicke states [33–35]. Therefore, we restrict our analysis to two special cases which can be treated with reasonable numerical efforts. The first case includes a single-photon Fock state, which simplifies the description since only one k -point transition can be excited. The second case involves a two-photon Fock state, which allows for all material states in which one or two k -point transitions are excited.

Below we present simplified equations for the respective special cases. In the case of a single photon, the basis set is reduced to

$$B_{\text{sp}} = \{|(v), 1\rangle, |(v|\gamma_1 = c), 0\rangle, |(v|\gamma_2 = c), 0\rangle, \dots, |(v|\gamma_N = c), 0\rangle\}, \quad (13)$$

resulting in the following equations of motion:

$$\partial_t c_1^{(v)} = \frac{i}{\hbar} \sum_{l=1}^N M_{kl} c_0^{(v|\gamma_l=c)} e^{-\frac{i}{\hbar} \Delta_{kl} t}, \quad (14)$$

$$\partial_t c_0^{(v|\gamma_j=c)} = \frac{i}{\hbar} M_{kj} c_1^{(v)} e^{\frac{i}{\hbar} \Delta_{kj} t}. \quad (15)$$

In this case, the observables read

$$O_{\text{ground}} = |c_1^{(v)}|^2, \quad (16)$$

$$O_c^{kj} = |c_0^{(v|\gamma_j=c)}|^2. \quad (17)$$

For an approximate description considering a parabolic dispersion near the vicinity of the band gap, the mentioned equations of motion are similar to the ones used in Ref. [36], where an inverse situation, namely, spontaneous emission near the edge of a photonic band gap, was investigated.

In the case of a two-photon Fock state, the basis set reads

$$B_{\text{tp}} = \{|(v), 2\rangle, |(v|\gamma_1 = c), 1\rangle, |(v|\gamma_2 = c), 1\rangle, \dots, |(v|\gamma_N = c), 1\rangle, |(v|\gamma_1 = \gamma_2 = c), 0\rangle, |(v|\gamma_1 = \gamma_3 = c), 0\rangle, \dots, |(v|\gamma_{N-1} = \gamma_N = c), 0\rangle\}. \quad (18)$$

Using the basis set, the equations of motion can be reduced to

$$\partial_t c_2^{(v)} = \frac{i}{\hbar} \sum_{l=1}^N M_{kl} c_1^{(v|\gamma_l=c)} e^{-\frac{i}{\hbar} \Delta_{kl} t} \sqrt{2}, \quad (19)$$

$$\begin{aligned} \partial_t c_1^{(v|\gamma_j=c)} &= \frac{i}{\hbar} M_{kj} c_0^{(v)} e^{\frac{i}{\hbar} \Delta_{kj} t} \sqrt{2} \\ &+ \frac{i}{\hbar} \sum_{l=1, l \neq j}^N M_{kl} c_0^{(v|\gamma_l=\gamma_l=c)} e^{-\frac{i}{\hbar} \Delta_{kl} t}, \end{aligned} \quad (20)$$

$$\begin{aligned} \partial_t c_0^{(v|\gamma_j=\gamma_l=c)} &= \frac{i}{\hbar} M_{kj} c_1^{(v|\gamma_l=c)} e^{\frac{i}{\hbar} \Delta_{kj} t} \\ &+ \frac{i}{\hbar} M_{kl} c_1^{(v|\gamma_j=c)} e^{\frac{i}{\hbar} \Delta_{kl} t}. \end{aligned} \quad (21)$$

Then, the observables read

$$O_{\text{ground}} = |c_2^{(v)}|^2, \quad (22)$$

$$O_c^{kj} = |c_1^{(v|\gamma_j=c)}|^2 + \sum_{l=1, l \neq j}^N |c_0^{(v|\gamma_j=\gamma_l=c)}|^2. \quad (23)$$

III. ANALYTICAL TREATMENT

The analytical treatment of the system is based on the quasienergy approach, where we restrict our analysis to a resonant excitation condition ($\omega_g = \nu$) and a single-photon Fock state. We begin the analytical treatment with the eigenvalue problem for the Hamiltonian given in Eq. (1) that is evaluated in the basis set given in Eq. (13):

$$\hat{H} |\psi\rangle = \lambda |\psi\rangle, \quad (24)$$

where λ are eigenvalues (quasienergies) and we neglect a constant energy which is the same for all states and does not contribute to the dynamics. Calculating the determinant of the matrix corresponding to Eq. (24) and setting this determinant to zero, the following equation can be obtained:

$$-\lambda = M^2 \sum_{j=1}^N \frac{1}{\Delta_j - \lambda} =: G(\lambda). \quad (25)$$

Note that this expression is defined only for $M \neq 0$ since in the special case $M = 0$, the eigenvalues λ_i exactly equal the detunings Δ_i , resulting in a division by zero. Henceforth, we consider the case $M > 0$. Subsequently, the normalized eigenvectors read

$$|\psi_l\rangle = \frac{1}{\sqrt{1 + G'(\lambda_l)}} \left[|(v), 1\rangle + \sum_{j=1}^N \frac{M}{\Delta_j - \lambda_l} |(v|\gamma_j = c), 0\rangle \right]. \quad (26)$$

The state vector $|\Psi(t)\rangle$ can be written as an expansion with coefficients $z_l = \langle \psi_l | \Psi(t=0) \rangle$ with respect to the eigenbasis $\{|\psi_l\rangle\}$:

$$|\Psi(t)\rangle = \sum_l z_l e^{-\frac{i}{\hbar} \lambda_l t} |\psi_l\rangle. \quad (27)$$

Using this expansion and taking into account the initial condition $c_1^{(v)}(t=0) = 1$, the ground-state probability amplitude can be written as

$$c_1^{(v)} = \langle (v), 1 | \Psi \rangle = \sum_{j=0}^N \frac{e^{-\frac{i}{\hbar} \lambda_j t}}{1 + G'(\lambda_j)} = \sum_{j=0}^N w_j e^{-\frac{i}{\hbar} \lambda_j t}, \quad (28)$$

where we identified the weight of the quasienergy λ_j as

$$w_j = [1 + G'(\lambda_j)]^{-1}. \quad (29)$$

From Eq. (25) we can show that the spectrum of eigenvalues is composed of a single negative eigenvalue and a set of N positive eigenvalues, when counted according to their algebraic multiplicity; see the Appendix for details. Therefore, Eq. (28) can be decomposed as

$$c_1^{(v)} = w_0 e^{\frac{i}{\hbar} |\lambda_0| t} + \sum_{j=1}^N w_j e^{-\frac{i}{\hbar} |\lambda_j| t}. \quad (30)$$

In addition, using Eq. (25), we can also show that the spectrum of positive eigenvalues follows the band-structure profile; see the Appendix for details. Physically, such a separation into one negative and many positive eigenvalues is an analog of the situation of having one joint ground state expressing all the electrons in their valence bands (negative eigenvalue) and several possibilities to have electrons in an excited state. In

other words, we can talk about a collective excitation whose shape is determined by the band structure and is reflected in the spectrum of positive eigenvalues.

The second summand on the right-hand side of Eq. (30) is a superposition of N weighted oscillations with frequencies $-|\lambda_j|/\hbar$. For a large number of oscillations, $N \rightarrow \infty$, the sum can be approximated by an integral and can be identified as the Fourier transform of the continuous spectrum. According to the Riemann-Lebesgue lemma [37], the Fourier transform of a spectrum to the time domain becomes smaller over time and vanishes for $t \rightarrow \infty$. The first summand does not belong to the mentioned continuum and therefore remains unaffected. Thus, at the limit of large times, the ground-state probability is solely determined by the weight of the negative eigenvalue:

$$\lim_{t \rightarrow \infty} |c_1^{(v)}|^2 = |w_0|^2. \quad (31)$$

This property can also be shown explicitly by approximating the tight-binding band structure with parabolic functions and, further, for each parabolic function proceeding with the approach presented in Ref. [38].

In the following, the analytical treatment is divided into the 1D and 2D cases.

A. One-dimensional case

We start the analytical treatment with the 1D tight-binding band structure given by Eq. (8). First, by assuming a large number of k points, $N \rightarrow \infty$, we evaluate $G(\lambda)$ from Eq. (25) by replacing the sum with an integral. This integral can be calculated explicitly and used as a good approximation for calculating the negative eigenvalue:

$$G(\lambda) = M_0^2 \frac{a}{2\pi} \int_{-\pi/a}^{\pi/a} \frac{1}{\frac{\omega_b}{2}[1 - \cos(ka)] - \lambda} dk \quad (32)$$

$$= -M_0^2 \frac{1}{\lambda \sqrt{1 - \frac{\omega_b}{\lambda}}}, \quad \lambda < 0. \quad (33)$$

Substituting this expression in Eq. (25), we can find the negative eigenvalue, which in the case of $\omega_b \gg \lambda_0$ has a simple form:

$$\lambda_0 \approx -\left(\frac{M_0^4}{\omega_b}\right)^{1/3}, \quad 1 - \frac{\omega_b}{\lambda_0} \approx -\frac{\omega_b}{\lambda_0}. \quad (34)$$

The derivative of $G(\lambda)$ required for Eq. (29) can be calculated as

$$G'(\lambda) = -M_0^2 \frac{\omega_b - 2\lambda}{2\lambda^2(\lambda - \omega_b)\sqrt{1 - \frac{\omega_b}{\lambda}}}. \quad (35)$$

Generally, Eq. (25) with the use of $G(\lambda)$ defined in Eq. (33) has four roots, but only one of them is real and negative, which proves the statement made early about the existence of exactly one negative eigenvalue, independent of parameter choices. Equations (33) and (34) also demonstrate that M_0 , i.e., the light-matter interaction, is the only parameter which defines the negative eigenvalue when the band structure described by ω_b is fixed.

Figure 1 shows $|w_0|^2$ obtained from Eqs. (29) and (35) using two different approaches calculating λ_0 . The first approach utilizes the analytical solution from Eq. (34), which,

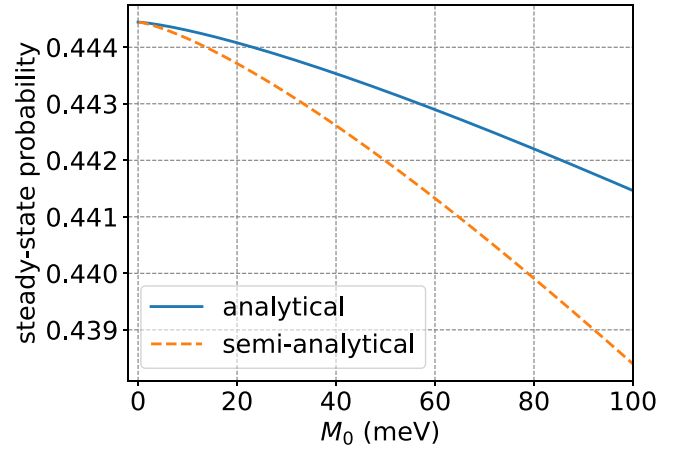


FIG. 1. Steady-state probability $|w_0|^2$ as a function of the light-matter coupling M_0 for the 1D tight-binding model obtained from Eq. (29) with Eq. (35). The solid blue curve is obtained by using the analytical solution for λ_0 from Eq. (34), while the dashed orange curve is obtained by solving $G(\lambda_0) = -\lambda_0$ numerically based on Eq. (33). The bandwidth is $\hbar\omega_b = 1.8$ eV. At the initial moment of time, the semiconductor is in the electronic ground state. The bandwidth and the initial condition are fixed for all other plots.

however, is decreasingly accurate for larger M_0 . Therefore, another curve is shown where λ_0 is obtained numerically based on Eq. (33). We see that both approaches lead to a similar result, which stresses the suitability of the analytical method from Eq. (34) for a solution. Furthermore, one can observe that in the 1D case, the choice of M_0 only slightly influences the final value of the GSP, which is in the range of 0.44. Note that the presented steady state appears due to taking into account a large number of k points and is formed in the limit of long times. A decrease in the coupling strength M_0 leads to an increased wait time for the steady state to form. In the limit $M_0 \rightarrow 0$ the system has very slow dynamics, which means that the steady state can be formed only after infinitely long wait times. Therefore, for a fixed observation time interval, the steady state will tend to 1 as $M_0 \rightarrow 0$. Note that the considered values for M_0 can be realized with proper cavities, as a reduction of the quantization volume leads to stronger coupling strengths according to $M_0 \sim \frac{1}{\sqrt{V}}$. Different microcavity systems that are suitable for such a realization are discussed in Ref. [39].

Analytical expressions for positive eigenvalues can be obtained by approximating the tight-binding band structure with parabolic functions and applying the approach presented in Ref. [38]. However, to avoid lengthy expressions and to make the representation clearer, we will proceed with a numerical solution to the eigenvalue problem stated in Eq. (24). The corresponding weights given by Eq. (29) are shown in Fig. 2, where in Figs. 2(a) and 2(b) we can clearly see the presence of one negative eigenvalue and the continuum of positive eigenvalues. Figure 2(c) shows the positive eigenvalues λ_j over the discretization index j , which results in a cosine dependence. This stresses the conclusion made in the previous section, i.e., that the spectrum of the positive eigenvalues follows the electronic band structure, even though they do not coincide.

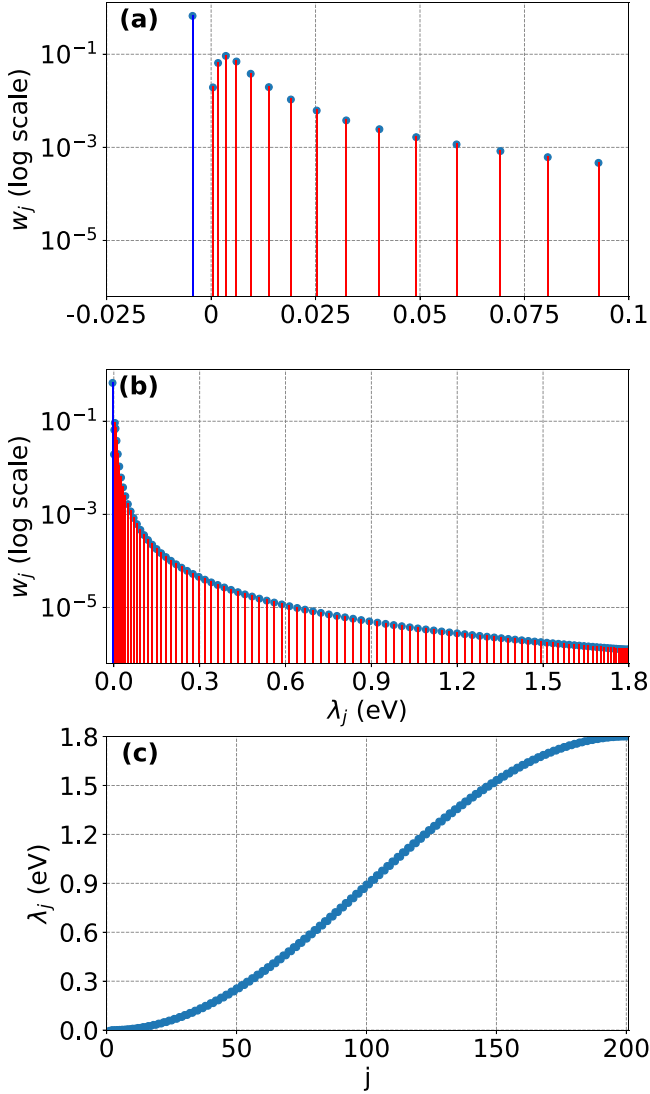


FIG. 2. Numerically computed weights of the eigenvalues in the case of the 1D tight-binding band structure for an energy range of (a) -0.025 to 0.1 eV and (b) -0.025 to 1.8 eV. (c) Eigenvalues are shown depending on their index j . The number of k points is $N = 200$ and $M_0 = 20$ meV.

B. Two-dimensional case

Next, we consider the 2D case with the band structure given by Eq. (9). Like in the previous section, we start by calculating $G(\lambda)$ and derive an approximate solution for λ_0 :

$$G(\lambda) = M_0^2 \int_{-\pi/a}^{\pi/a} \int_{-\pi/a}^{\pi/a} \frac{[a/(2\pi)]^2 dk_x dk_y}{\frac{\omega_b}{4} [2 - \cos(k_x a) - \cos(k_y a)] - \lambda} \quad (36)$$

$$= \frac{M_0^2}{\pi} \sqrt{\frac{4}{\lambda(\lambda - \omega_b)}} K\left(-\frac{\omega_b^2}{4\lambda(\lambda - \omega_b)}\right), \quad \lambda < 0, \quad (37)$$

$$\Rightarrow \lambda_0 \approx -\frac{2M_0^2}{\pi\omega_b} W\left(\frac{2\pi\omega_b^2}{M_0^2}\right), \quad 1 - \frac{\omega_b}{\lambda_0} \approx -\frac{\omega_b}{\lambda_0}, \quad (38)$$

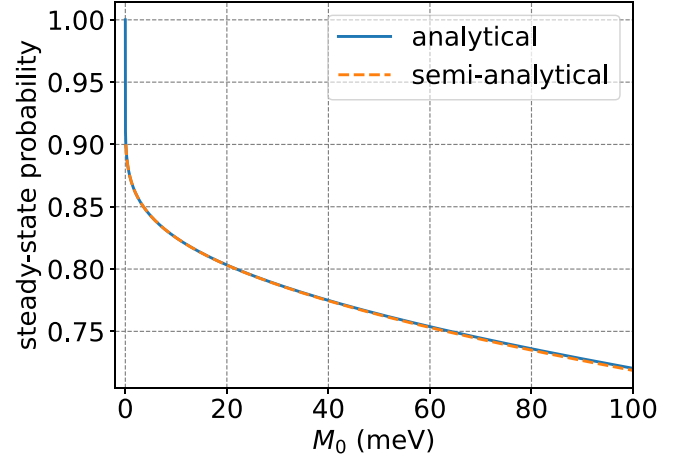


FIG. 3. Steady-state probability $|w_0|^2$ as a function of the light-matter coupling M_0 for the 2D tight-binding model obtained from Eq. (29) with the use of Eq. (39). The solid blue curve is obtained by using the analytical solution for λ_0 from Eq. (38), while the dashed orange curve is obtained by solving $G(\lambda_0) = -\lambda_0$ numerically based on Eq. (37).

$$G'(\lambda) = \frac{1}{\pi(\omega_b - 2\lambda)} 4M_0^2 \sqrt{\frac{1}{\lambda(\lambda - \omega_b)}} E\left(-\frac{\omega_b^2}{4\lambda(\lambda - \omega_b)}\right), \quad (39)$$

where $K(m)$ denotes the complete elliptic integral of the first kind, $E(m)$ denotes the complete elliptic integral of the second kind [40], and $W(z)$ is the Lambert W function [41].

This calculation was performed analogously to the one in the 1D case and allows us to compute the weight of the negative eigenvalue analytically according to Eq. (29) using Eqs. (38) and (39). The presented expressions again demonstrate the existence of exactly one negative eigenvalue despite the choice of parameters.

Figure 3 shows $|w_0|^2$ from Eq. (29) with the use of Eq. (39) depending on M_0 . Here, we apply the same procedure as before; that is, we obtain λ_0 from the analytical solution (38) and from numerically solving $G(\lambda_0) = -\lambda_0$ with Eq. (37). In contrast to the 1D case, such a dependence is more pronounced and is found to be at larger values of the steady-state probability. The latter is explained by the increase in k points, compared to 1D case, that are excited nonresonantly. A total excitation of such k points is more inefficient than in the 1D case, resulting in less total conduction-band occupation.

We proceed with a numerical demonstration of positive eigenvalues by solving the eigenvalue problem (24) (see Fig. 4, where the red stripes were omitted for better visibility). While the structure of the solution is more complex than in the 1D case, the eigenvalues can again be decomposed into a dominating negative eigenvalue and a continuum of positive eigenvalues according to Eq. (30). Therefore, regardless of the dimensionality of the problem, the ground-state probability is determined by the negative eigenvalue.

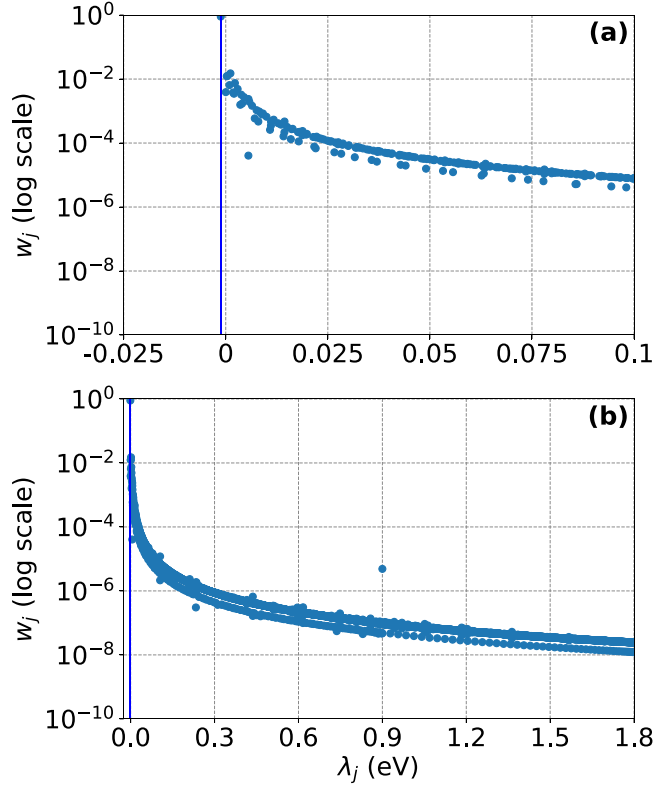


FIG. 4. Numerically computed eigenvalues in the case of the 2D tight-binding band structure for an energy range of (a) -0.025 to 0.1 eV and (b) -0.025 to 1.8 eV. The number of k points is $N = 201$ per dimension, $M_0 = 20$ meV.

IV. NUMERICAL SIMULATIONS

After analyzing the eigenvalue problem defined by the Hamiltonian, we proceed with numerical simulations of the equations of motion (5). This allows us a more effective treatment of nonresonant excitations and a detailed view into the dynamics in the conduction band. The numerical analysis again is divided into the 1D and 2D cases. Unless stated otherwise, the presented results are computed for the single-photon case.

A. One-dimensional case

For the 1D case, we fix $M_0 = 20$ meV as a model parameter and start with the consideration of resonant excitation conditions. The conduction-band occupations $O_c^{k_j}$ and the GSP are shown in Figs. 5(a) and 5(b), respectively. The conduction-band occupations for the respective k points can be identified as oscillations with different frequencies, which are approximately the optical detunings Δ_k . Due to the conservation of the trace, the GSP O_{ground} can be directly connected to the conduction-band occupation $O_c^{k_j}$ as

$$O_{\text{ground}} = 1 - \sum_{j=1}^N O_c^{k_j}. \quad (40)$$

It can be seen that, despite the rich dynamics of each k point over time, the sum of conduction-band occupations for all k points leads to a constant probability value corresponding to a

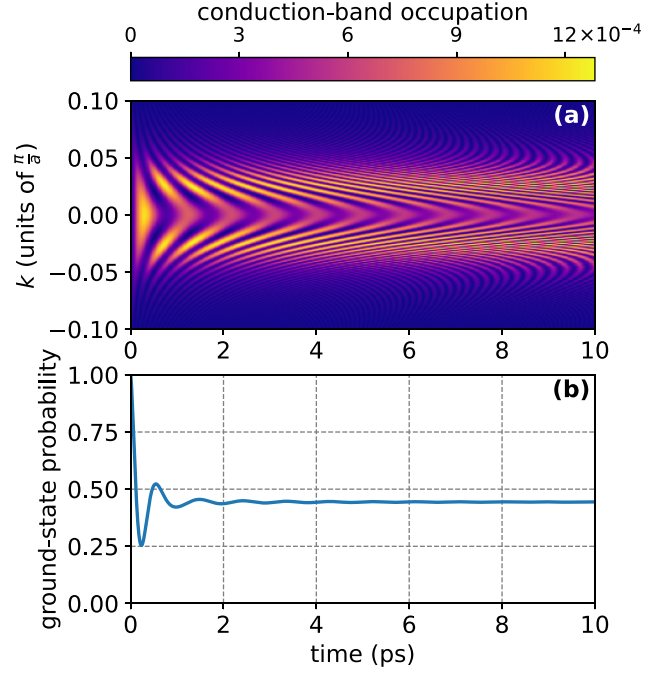


FIG. 5. (a) Conduction-band occupation and (b) GSP for the 1D tight-binding model with $M_0 = 20$ meV; the number of k points is $N = 20001$.

collective excitation of a semiconductor, which, according to Eq. (40), is reflected in a constant value of the GSP at large times. We find this steady-state value of GSP to be around 0.44, as predicted by the analytical treatment based on the eigenvalue problem.

As a next step, we consider nonresonant excitation conditions. For this, we introduce the energetic offset $\delta = \hbar(\nu - \omega_g)$, where $\delta > 0$ leads to an excitation inside the band structure since the light mode is energetically above the band gap, whereas $\delta < 0$ is an optical excitation below the band-gap energy. The conduction-band occupation for different energetic offsets δ is presented in Fig. 6.

Comparing Figs. 6(a) and 6(b), which show the cases of $\delta = -5$ meV and $\delta = 0$ meV, respectively, we can see that an excitation of the semiconductor below the band-gap energy $\delta < 0$ leads to faster oscillations with smaller amplitudes compared to the resonant excitation, which physically is explained by the increased optical detuning Δ_{k_j} for each respective k point. In contrast, $\delta > 0$ leads to the formation of two stripes, approximately found at $\Delta_{k_j} = 0$; see Figs. 6(c) and 6(d), which show the cases for $\delta = 6$ meV and $\delta = 10$ meV, respectively. This behavior is led back to eigenstates that correspond to positive eigenvalues and are energetically located inside the conduction band being excited resonantly. Such a resonant excitation of various k -point transitions inside the conduction band leads to the formation of a steady state, where the occupation is stored inside the conduction band.

With the described behavior, the dynamics of the GSP shown in Fig. 7 can be easily understood. Indeed, negative energetic offsets, which lead to a weak-weighted continuum that oscillates faster, lead to a higher GSP that also oscillates faster than the resonant excitation condition. In contrast, pos-

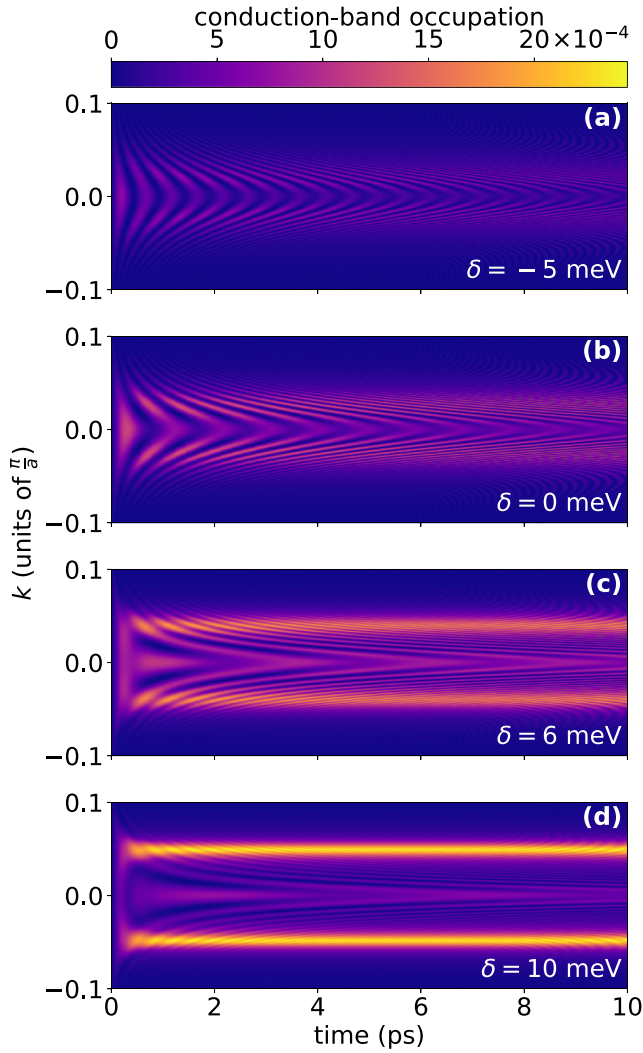


FIG. 6. Conduction-band occupation for the 1D tight-binding model for $M_0 = 20$ meV, $N = 20\,001$, and (a) $\delta = -5$ meV, (b) $\delta = 0$ meV, (c) $\delta = 6$ meV, and (d) $\delta = 10$ meV.

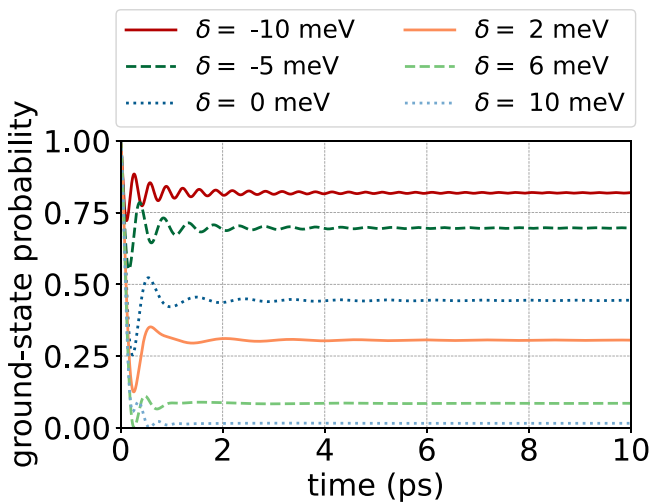


FIG. 7. GSP for the 1D tight-binding model with $M_0 = 20$ meV, $N = 20\,001$ for different energetic offsets δ .

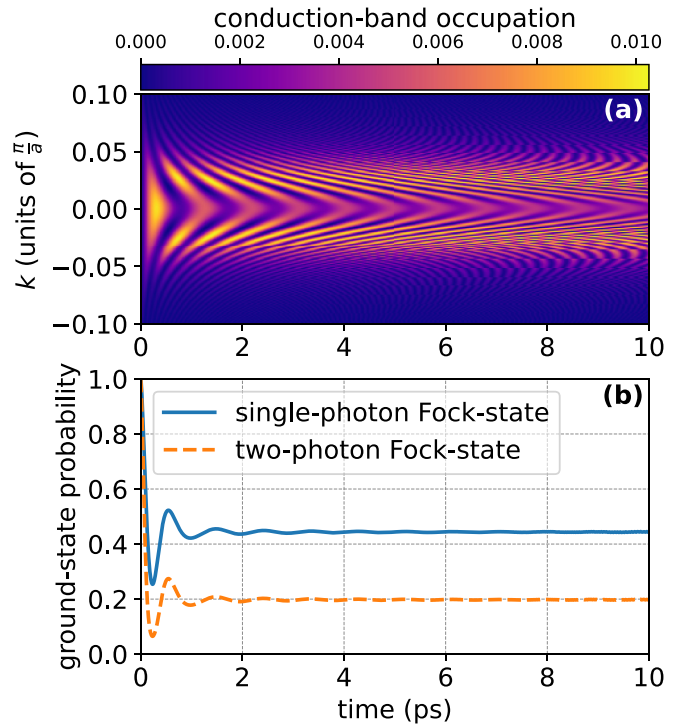


FIG. 8. (a) Conduction-band occupation for a two-photon excitation. (b) GSP for the single-photon Fock-state ($N = 5001$) and the two-photon Fock-state ($N = 5001$) excitations, $M_0 = 20$ meV.

itive energetic offsets, which result in occupation trapping in eigenstates corresponding to resonant excitation conditions, lead to a fast decay of the GSP, eventually approaching zero for large enough δ .

We finalize the investigation of the 1D case with a consideration of a two-photon Fock-state, which is of particular interest since it allows one to predict the behavior upon transition to states with a large number of photons. Figure 8(b) shows the GSP for an excitation with a two-photon Fock state together with the GSP for an excitation with a single-photon Fock state.

Compared with the single-photon case, the GSP for a two-photon excitation is located at much smaller values. This is caused by the large number of possible excitations that are introduced by using two photons, which is reflected in the basis states (18). The increased number of excitations reduces the possibility that all k points will be unexcited. Thus, one can predict that multiphoton states will generally lead to a smaller GSP. Furthermore, it is to be expected that the GSP will be zero in most semiclassical treatments, where light is composed of thousands of photons, making it unlikely to find no electronic excitations at any point in time. Figure 8(a) shows the conduction-band occupation distribution for a two-photon excitation. Such a distribution qualitatively resembles the single-photon case shown in Fig. 5(a); however, its magnitude is generally higher since a two-photon excitation gives rise to more possible electronic excitations. Note that due to the trace conservation, the absolute value of the conduction-band occupation distribution depends on the number of k points; however, the normalized profile of

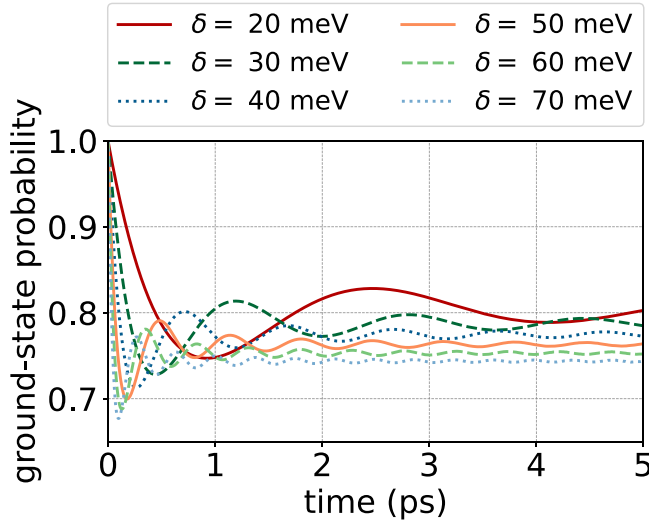


FIG. 9. GSP for the 2D tight-binding model with $N = 2000$ k points per dimension and different coupling constants M_0 depicted in the legend.

distribution is k independent; therefore, the recent conclusion is valid regardless of the number of considered k points.

B. Two-dimensional case

As concluded in the analytical treatment, the 2D tight-binding band structure, on the one hand, shares properties with the 1D tight-binding band structure, like the overall structure of the eigenvalue spectrum, but, on the other hand, shows fundamentally different properties, such as its dependence on the light-matter coupling M_0 . Thus, we begin the numerical analysis of the resonantly excited 2D case with simulations of the dynamics for different M_0 (see Fig. 9).

As in the case of the 1D tight-binding model, the parameter M_0 determines the timescale of the system dynamics. But in contrast to the 1D case, different values of M_0 lead to a visible change in the mean value of the GSP. However, apart from this, the overall form of the GSP dynamics is still similar to the 1D case, and therefore, general properties pointed out in this work will be valid for different choices of M_0 . As already pointed out in the analytical treatment, the overall value of the GSP in the 2D case is higher than in the 1D case since the nonresonantly excited k points are weighted more strongly; for a comparison see the curves for $M_0 = 20$ meV in Figs. 9 and 5(b).

Next, we consider nonresonant excitation conditions, i.e., $\delta \neq 0$, and fix $M_0 = 50$ meV as a model parameter. Figure 10 depicts the GSP for different δ . One can note that the qualitative behavior of the GSP for different detunings is similar to that in the 1D case. However, in the 2D case, the conduction-band occupation corresponds to a 2D grid and has more complex dynamics.

Figure 11 shows the conduction-band occupation for the 2D case, where Figs. 11(a) and 11(c) are the time dynamics for a cut at $k_x = 0$, while Figs. 11(b) and 11(d) show the conduction-band occupation on the full grid at $t = 1$ ps. Here, Figs. 11(a) and 11(b) depict the resonant case ($\delta = 0$ meV), and Figs. 11(c) and 11(d) depict a nonresonant case ($\delta =$

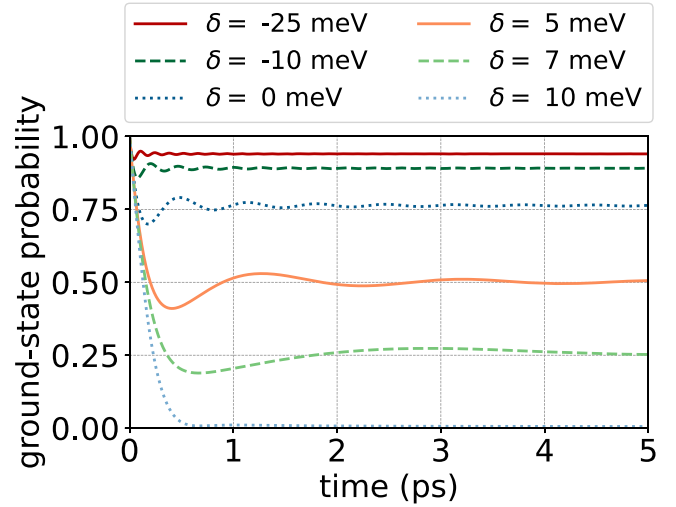


FIG. 10. GSP for the 2D tight-binding model with $M_0 = 50$ meV and $N = 2000$ k points per dimension for different energetic offsets δ .

50 meV). One can notice that the qualitative behavior of the conduction-band occupation is similar to that in the 1D case: with $\delta > 0$, the population is mostly trapped in the eigenstates corresponding to the positive eigenvalues; however, the shape of such collective excitations is different due to the different (2D) geometry of the band structure. In the 2D plane, the resonant excitation leads to the formation of circles, whose radii oscillate with time, whereas a nonresonant excitation leads to the formation of a circle with a fixed radius.

V. CONCLUSION

In this work, we presented a theoretical approach for a microscopic description of quantum-optically excited extended one- and two-dimensional semiconductor nanostructures where the photon statistics is fully taken into account. An analytical treatment that is based on the eigenvalue problem of the system yields detailed insight into the system's properties and allows for a deeper understanding of the occurring dynamics. We demonstrated that both the 1D and 2D tight-binding band structures have exactly one negative eigenvalue, which determines the steady state of the system, while the formed continuum of positive eigenvalues behaves similarly to the band structure, even though they are not identical.

In the numerical treatment of the system, when the dynamical equations of motion were solved, we showed that a collective excitation of the conduction-band occupation is formed during the dynamics. At long times, destructive interference within the continuum of positive eigenvalues of the system occurs, which results in a steady state for the occupation probability of the ground state. Due to the wide band structure, nonresonant band-gap excitation can become resonant with transitions at other k points, which leads to the formation of new steady states.

Furthermore, we demonstrated that an increase in the number of photons of quantum light (two-photon excitations) increases the occupation of the conduction band, while the ground-state probability decreases. The presented results for

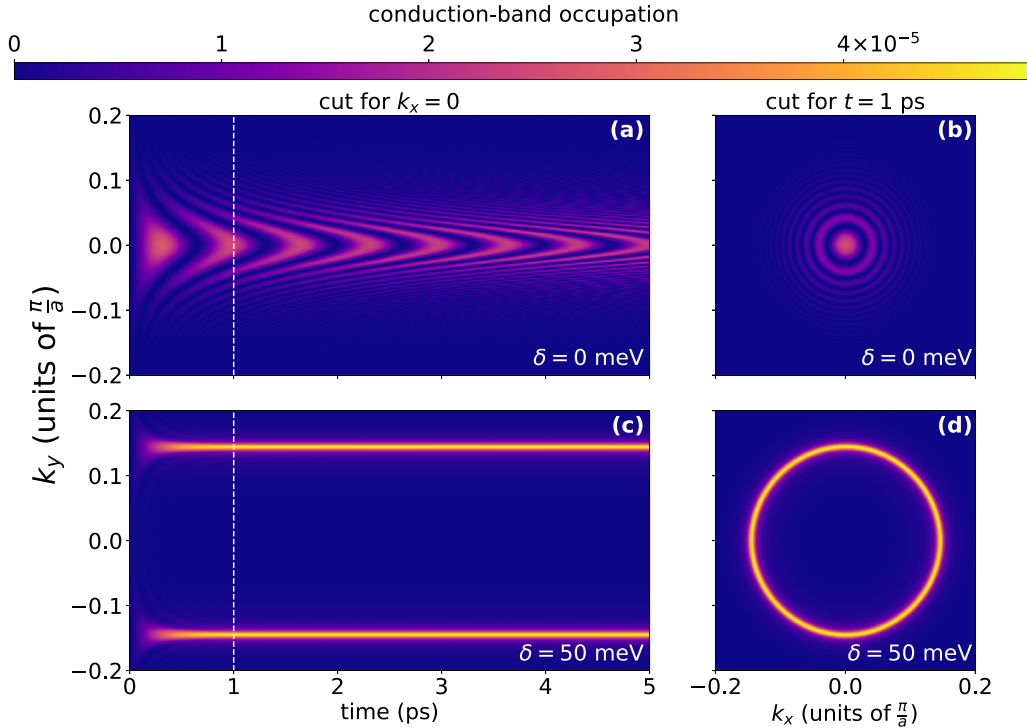


FIG. 11. Conduction-band occupation for the 2D tight-binding model with $M_0 = 50$ meV, $N = 2501$ k points per dimension, where (a) the cut at $k_x = 0$ and $\delta = 0$ meV, (b) the cut at $t = 1$ ps and $\delta = 0$ meV, (c) the cut at $k_x = 0$ and $\delta = 50$ meV, and (d) the cut at $t = 1$ ps and $\delta = 50$ meV are considered.

different cases show the consistency between the analytical and numerical treatments. An interesting extension to the current model is the inclusion of Coulomb interaction and the study of exciton or exciton-polariton states.

ACKNOWLEDGMENTS

A joint grant by the Deutsche Forschungsgemeinschaft (DFG) (Projects No. ME 1916/7-1 and No. SH 1228/2-1) and the Russian Science Foundation (RSF) (Grant No. 19-42-04105) and support by the DFG through the Collaborative Research Center TRR 142/3 (Project No. 231447078, Subproject A02) is gratefully acknowledged. We are thankful for a computation time grant provided by the Paderborn Center for Parallel Computing (PC²).

APPENDIX: STRUCTURE OF THE EIGENVALUE SPECTRUM

In the main text, we claimed that it follows from Eq. (25) that the eigenvalue spectrum is composed of exactly one negative eigenvalue and N positive eigenvalues when they are counted according to the algebraic multiplicity. In the following, we prove this. From Eq. (25) it follows that λ is a solution if the functions $f(\lambda) = -\lambda$ and $G(\lambda)$ intersect. We note that $G(\lambda)$ has singularities at $\lambda = \Delta_j$. Since $\Delta_j \geq 0$, we know that both G and f are well defined in the domain

$D = (-\infty, 0)$ and, especially, are differentiable. We calculate the first derivatives of the functions G and f to study their monotonous behavior:

$$f'(\lambda) = -1 < 0, \quad (\text{A1})$$

$$G'(\lambda) = M^2 \sum_{j=1}^N \frac{1}{(\Delta_j - \lambda)^2} > 0. \quad (\text{A2})$$

We conclude that f is a strictly monotonously decreasing function and G a strictly monotonously increasing function. For the domain $D = (-\infty, 0)$ we find that the range of f is $B_f = (0, \infty)$ and $G(\lambda) > 0$. Thus, the range of G is a subset of B_f , which is why exactly one solution exists in the domain D , i.e., there is exactly one negative eigenvalue. Since an $(N + 1) \times (N + 1)$ matrix has $N + 1$ eigenvalues when counted according to their algebraic multiplicity, the remaining N eigenvalues must be positive, which gives the claim.

The idea of this proof can be extended to domains between two adjacent singularities Δ_j and Δ_l , i.e., $D = (\Delta_j, \Delta_l)$, where one can show that the range of f is a subset of the range of G , which, together with the monotonous behavior, lets us conclude that there must exist a positive eigenvalue in the domain (Δ_j, Δ_l) . From this, one can conclude that the positive eigenvalue spectrum follows the form of the band structure.

- [1] M. O. Scully and M. S. Zubairy, *Quantum Optics* (Cambridge University Press, Cambridge, 1997).
- [2] S. Slussarenko and G. J. Pryde, Photonic quantum information processing: A concise review, *Appl. Phys. Rev.* **6**, 041303 (2019).
- [3] N. Gisin, G. Ribordy, W. Tittel, and H. Zbinden, Quantum cryptography, *Rev. Mod. Phys.* **74**, 145 (2002).
- [4] H.-S. Zhong, H. Wang, Y.-H. Deng, M.-C. Chen, L.-C. Peng, Y.-H. Luo, J. Qin, D. Wu, X. Ding, Y. Hu, P. Hu, X.-Y. Yang, W.-J. Zhang, H. Li, Y. Li, X. Jiang, L. Gan, G. Yang, L. You, Z. Wang, L. Li, N.-L. Liu, C.-Y. Lu, and J.-W. Pan, Quantum computational advantage using photons, *Science* **370**, 1460 (2020).
- [5] M. Kira and S. W. Koch, *Semiconductor Quantum Optics* (Cambridge University Press, Cambridge, 2012).
- [6] K. Jürgens, F. Lengers, D. Groll, D. E. Reiter, D. Wigger, and T. Kuhn, Comparison of the semiclassical and quantum optical field dynamics in a pulse-excited optical cavity with a finite number of quantum emitters, *Phys. Rev. B* **104**, 205308 (2021).
- [7] M. Kira and S. W. Koch, Cluster-expansion representation in quantum optics, *Phys. Rev. A* **78**, 022102 (2008).
- [8] C. W. J. Beenakker and H. van Houten, Quantum transport in semiconductor nanostructures, *Solid State Phys.* **44**, 1 (1991).
- [9] D. Bimberg, *Semiconductor Nanostructures* (Springer, Berlin, 2008).
- [10] A. N. Kosarev, H. Rose, S. V. Poltavtsev, M. Reichelt, C. Schneider, M. Kamp, S. Höfling, M. Bayer, T. Meier, and I. A. Akimov, Accurate photon echo timing by optical freezing of exciton dephasing and rephasing in quantum dots, *Commun. Phys.* **3**, 228 (2020).
- [11] F. P. García de Arquer, D. V. Talapin, V. I. Klimov, Y. Arakawa, M. Bayer, and E. H. Sargent, Semiconductor quantum dots: Technological progress and future challenges, *Science* **373**, 6555 (2021).
- [12] M. J. Stevens, A. Najmaie, R. D. R. Bhat, J. E. Sipe, H. M. van Driel, and A. L. Smirl, Optical injection and coherent control of a ballistic charge current in GaAs/AlGaAs quantum wells, *J. Appl. Phys.* **94**, 4999 (2003).
- [13] P.-C. Ku, F. Sedgwick, C. J. Chang-Hasnain, P. Palinginis, T. Li, H. Wang, S.-W. Chang, and S.-L. Chuang, Slow light in semiconductor quantum wells, *Opt. Lett.* **29**, 2291 (2004).
- [14] M. Jacquet, M. Joly, F. Claude, L. Giacomelli, Q. Glorieux, A. Bramati, I. Carusotto, and E. Giacobino, Analogue quantum simulation of the Hawking effect in a polariton superfluid, *Eur. Phys. J. D* **76**, 152 (2022).
- [15] M. J. Jacquet, L. Giacomelli, Q. Valnais, M. Joly, F. Claude, E. Giacobino, Q. Glorieux, I. Carusotto, and A. Bramati, Quantum vacuum excitation of a quasi-normal mode in an analog model of black hole spacetime, [arXiv:2110.14452](https://arxiv.org/abs/2110.14452).
- [16] W. W. Chow, S. W. Koch, and M. Sargent III, *Semiconductor-Laser Physics* (Springer, Berlin, 1994).
- [17] H. Haug and S. W. Koch, *Quantum Theory of the Optical and Electronic Properties of Semiconductors*, 4th ed. (World Scientific, Singapore, 2005).
- [18] S. V. Andreev, Dipolar polaritons squeezed at unitarity, *Phys. Rev. B* **101**, 125129 (2020).
- [19] T. Meier, P. Thomas, and S. W. Koch, *Coherent Semiconductor Optics: From Basic Concepts to Nanostructure Applications* (Springer, New York, 2007).
- [20] W.-R. Hannes and T. Meier, Higher-order contributions and nonperturbative effects in the nondegenerate nonlinear optical absorption of semiconductors using a two-band model, *Phys. Rev. B* **99**, 125301 (2019).
- [21] J. Kabuss, A. Carmele, M. Richter, and A. Knorr, Microscopic equation-of-motion approach to the multiphonon assisted quantum emission of a semiconductor quantum dot, *Phys. Rev. B* **84**, 125324 (2011).
- [22] A. Carmele, J. Kabuss, M. Richter, A. Knorr, and W. W. Chow, Quantum optics in a semiconductor quantum dot, *J. Mod. Opt.* **58**, 1951 (2011).
- [23] N. Bannov, V. Aristov, V. Mitin, and M. A. Stroschio, Electron relaxation times due to the deformation-potential interaction of electrons with confined acoustic phonons in a free-standing quantum well, *Phys. Rev. B* **51**, 9930 (1995).
- [24] P. Michler, A. Kiraz, C. Becher, W. V. Schoenfeld, P. M. Petroff, L. Zhang, E. Hu, and A. Imamoglu, A quantum dot single-photon turnstile device, *Science* **290**, 2282 (2000).
- [25] J. McKeever, A. Boca, A. D. Boozer, R. Miller, J. R. Buck, A. Kuzmich, and H. J. Kimble, Deterministic generation of single photons from one atom trapped in a cavity, *Science* **303**, 1992 (2004).
- [26] B. Darquié, M. P. A. Jones, J. Dingjan, J. Beugnon, S. Bergamini, Y. Sortais, G. Messin, A. Browaeys, and P. Grangier, Controlled single-photon emission from a single trapped two-level atom, *Science* **309**, 454 (2005).
- [27] P. Maunz, D. Moehring, S. Olmschenk, K. C. Younge, D. N. Matsukevich, and C. Monroe, Quantum interference of photon pairs from two remote trapped atomic ions, *Nat. Phys.* **3**, 538 (2007).
- [28] J.-H. An, M. Feng, and C. H. Oh, Quantum-information processing with a single photon by an input-output process with respect to low- Q cavities, *Phys. Rev. A* **79**, 032303 (2009).
- [29] A. Beveratos, R. Brouri, T. Gacoin, A. Villing, J. Poizat, and P. Grangier, Single Photon Quantum Cryptography, *Phys. Rev. Lett.* **89**, 187901 (2002).
- [30] K. J. Blow, R. Loudon, S. J. D. Phoenix, and T. J. Shepherd, Continuum fields in quantum optics, *Phys. Rev. A* **42**, 4102 (1990).
- [31] O. Tsyplatyev and D. Loss, Dynamics of the inhomogeneous Dicke model for a single-boson mode coupled to a bath of nonidentical spin-1/2 systems, *Phys. Rev. A* **80**, 023803 (2009).
- [32] O. Tsyplatyev and D. Loss, Classical and quantum regimes of the inhomogeneous Dicke model and its Ehrenfest time, *Phys. Rev. B* **82**, 024305 (2010).
- [33] M. Gegg, A. Carmele, A. Knorr, and M. Richter, Superradiant to subradiant phase transition in the open system Dicke model: Dark state cascades, *New J. Phys.* **20**, 013006 (2018).
- [34] M. Scheibner, T. Schmidt, L. Worschech, A. Forchel, G. Bacher, T. Passow, and D. Hommel, Superradiance of quantum dots, *Nat. Phys.* **3**, 106 (2007).
- [35] N. Shammah, S. Ahmed, N. Lambert, S. De Liberato, and F. Nori, Open quantum systems with local and collective incoherent processes: Efficient numerical simulations using permutational invariance, *Phys. Rev. A* **98**, 063815 (2018).
- [36] S. John and T. Quang, Spontaneous emission near the edge of a photonic band gap, *Phys. Rev. A* **50**, 1764 (1994).
- [37] S. Bochner and K. Chandrasekharan, *Fourier Transforms* (Princeton University Press, Princeton, NJ, 1949).
- [38] H. Rose, A. N. Vasil'ev, O. V. Tikhonova, T. Meier, and P. R. Sharapova, Excitation of an electronic band structure

- by a single-photon Fock state, Zenodo, <https://doi.org/10.5281/zenodo.5774986>.
- [39] D. S. Dovzhenko, S. V. Ryabchuk, Y. P. Rakovich, and I. R. Nabiev, Light-matter interaction in the strong coupling regime: Configurations, conditions, and applications, *Nanoscale* **10**, 3589 (2018).
- [40] *Handbook of Mathematical Functions with Formulas, Graphs, and Mathematical Tables*, edited by M. Abramowitz and I. A. Stegun (Dover, New York, 1972).
- [41] R. M. Corless, G. H. Gonnet, D. E. G. Hare, D. J. Jeffrey, and D. E. Knuth, On the Lambert W function, *Adv. Comput. Math.* **5**, 329 (1996).